Hindawi
Mathematical Problems in Engineering
Volume 2018, Article ID 7824671, 15 pages
https://doi.org/10.1155/2018/7824671

Research Article

Match-Mode Autoregressive Method for Moving Source Depth Estimation in Shallow Water Waveguides

Liang Guo-Long,[1,2,3] Zhang Yi-Feng,[1,2,3] Zou Nan ,[1,2,3] and Wang Jin-Jin[1,2,3]

[1] *Acoustic Science and Technology Laboratory, Harbin Engineering University, Harbin 150001, China*
[2] *Key Laboratory of Marine Information Acquisition and Security (Harbin Engineering University), Ministry of Industry and Information Technology, Harbin 150001, China*
[3] *College of Underwater Acoustic Engineering, Harbin Engineering University, Harbin 150001, China*

Correspondence should be addressed to Zou Nan; zounan@hrbeu.edu.cn

Received 23 November 2018; Accepted 16 December 2018; Published 31 December 2018

Academic Editor: Francesco Aymerich

Source depth estimation is always a problem in underwater acoustic area, because depth estimation is a nonlinear problem. Traditional depth estimation methods use a vertical line array, which has disadvantage of poor mobility due to the size of sensor array. In order to estimate source depth with a horizontal line array, we propose a matched-mode depth estimation method based on autoregressive (AR) wavenumber estimation for a moving source in shallow water waveguides. First, we estimate the mode wavenumbers using the improved AR modal wavenumber spectrum. Second, according to the mode wavenumber estimation, we estimate the mode amplitudes by the wavenumber spectrum, which is obtained by generalized Hankel transform. Finally, we estimate source depth estimation by the peak of source depth function wherein the data mode best matches the replica mode that is calculated using a propagation model. Compared with synthetic aperture beamforming, the proposed method exhibits a better performance in source depth estimation under low signal-to-noise ratio or the small range span. The robustness of the proposed method is illustrated by simulating the performance in mismatched environment.

1. Introduction

Matched field processing (MFP) [1–3] is a popular method for localizing the source in complex propagation environments. Conventional MFP obtains the range depth function, that is, the correlation between the replica and the measured fields. The source location is determined by the peak of the range depth function. MFP can localize source accurately in a range-independent or slowly varying environment without considering any environmental mismatches. However, when the sound propagation is not exactly modeled, the range and depth estimated by MFP generally present an error, which is referred to as the environmental mismatch problem [4]. The need for depth estimation is more pressing than range estimation for some applications. The source range and depth are estimated simultaneously by MFP, which indicates that depth estimation depends on range estimation. The robustness of depth estimation decreases because of the sensitivity of range estimation to sound speed profile (SSP). MFP always requires a vertical line array (VLA) or horizontal line array (HLA) with large aperture. However, real application of large aperture array is difficult because of the installation platform. The application of MFP is restricted by the aperture problem and the environmental mismatch problem. Consequently, an active area of research in recent years has been devoted to estimate source depth robustly by a single sensor or a short line array [5–8].

A class of methods that has shown some promise in passive location exploits the properties of the reliable acoustic path (RAP) [8]. Such methods reduce the requirement of array aperture. The difficulty associated with the propagation of RAP limits the application of the method in shallow water. Depth estimation for shallow water waveguides is generally performed in two steps: mode filtering first and then MMP [3]. The modal amplitudes are determined by mode filters, and then MMP is used to estimate the source location based on the modal amplitude estimation. However, the mode filters always require well-sampling of the water

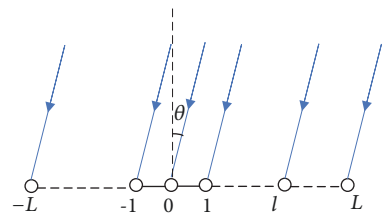

Figure 1: Array receiving schematic.

column by the VLA; otherwise, the mode filtering will become an ill-posed problem. The difficulty in source depth estimation using a short line array is the lack of spatial information. Therefore, some previous studies have relied on the multifrequency characteristics of wideband signals in estimating source depth [9, 10]. Considering the dispersion phenomenon of signals in shallow water, some scholars have estimated source depth on the basis of the related information of marine environment contained in dispersion [11]. However, the aforementioned studies have restricted the signal form to be broadband and few works on source depth estimation for signal with low-frequency line spectrum are available. Recently, data-based MMP is being proposed for a moving source by using a full-spanning VLA, which is free of the environmental mismatch problem in theory [12, 13]. Yang [7] proposed a method based on the idea of data-based MMP to estimate moving source depth, and this method requires only a single hydrophone. It is more robust than MFP for depth estimation because of not requiring source range estimation. However, the method presents an inherent drawback. The method requires source traveling a sufficient range in radial direction owing to that the mode wavenumbers are estimated by synthetic aperture modal beamforming (SAB). Some of the horizontal wavenumbers cannot be estimated, when the moving range does not meet the requirement. Source depth estimation based on synthetic aperture beaming may be incorrect.

T.C. Yang mentioned the issue and presented the high resolution algorithms to solve this issue [12]. Following his idea, we propose a source depth estimation approach with a HLA for a moving source in a range-independent environment, without knowing source absolute range information in this study. When beam steers to the source direction, the signal is enhanced after beamforming. We apply the autoregressive (AR) model to the signal enhanced by array gain to estimate the wavenumbers. The AR wavenumber spectrum is unsuitable to estimate mode amplitudes. Therefore, the generalized Hankel transform is applied to the data. The source depth is estimated by the peak of the depth ambiguity function wherein the mode depth functions best match the mode amplitudes. Compared with SAB, the proposed method effectively improves the depth estimation performance for the data with short range span or low SNR, and exhibits better adaptability to the notion of the observation platform. In addition, the proposed method can be applied to underwater unmanned vehicles or the autonomous underwater vehicles because it identifies the peaks of wavenumber spectrum automatically.

The remainder of the paper is organized as follows. The wavenumber estimation for the beamforming output is developed in Section 2. In Section 2.1, the generalized Hankel transform is extended to beamforming output in a range-independent environment [7]. A method for wavenumber estimation based on an AR model without knowing the source range is proposed in Section 2.2. Source depth estimation based on wavenumber spectrum is introduced in Section 3. The factors that influence the performance of the algorithm are explored in Section 4. The performance of the algorithm on the data with different SNRs and different range spans is analyzed in Section 4.1. The performance of the algorithm in mismatch environment is evaluated in Section 4.2. A summary and discussion is provided in Section 5.

2. Mode Wavenumber Estimation

We assume that source travels at a fixed depth during observation in a range-independent environment. The considered HLA possesses $2L+1$ receivers that are uniformly spaced with d as shown in Figure 1.

The range between source and the center of HLA is r_i at the ith moment. The far-field source radiates the continuous wave signal, with a look direction θ_i. θ_i is the true value of the look direction at the ith moment. In shallow water waveguides, we suppress a time dependence of the form $e^{j\omega t}$ with ω positive; therefore, the pressure field of the sensor l at the ith moment can be represented using normal mode theory as

$$p_l(r_i, z_r) = \sqrt{2\pi} e^{-j(\pi/4)} \sum_{m=1}^{M} \phi_m(z_s)\, \phi_m(z_r) \cdot \frac{\exp\{-j(k_m - j\alpha_m)[r_i + ld\sin\theta_i]\}}{\sqrt{k_m[r_i + ld\sin\theta_i]}}, \tag{1}$$

where k_m, α_m, and ϕ_m are the wavenumber, the attenuation coefficient, and the mode depth function, respectively, which all belong to the mth mode; z_s and z_r are the source and HLA depths, respectively; and M is the number of modes considered in the propagation model.

The source is at the far field, such that $r_i + ld\sin\theta_i \approx r_i$. Equation (1) is simplified as

$$p_l(r_i, z_r) = \sqrt{2\pi} e^{-j(\pi/4)} \sum_{m=1}^{M} \phi_m(z_s)\, \phi_m(z_r)$$

$$\cdot \frac{\exp\{-j(k_m - j\alpha_m)[r_i + ld\sin\theta_i]\}}{\sqrt{k_m r_i}} = \sum_{m=1}^{M} A_m \exp\{-j(k_m - j\alpha_m)[r_i + ld\sin\theta_i]\}, \tag{2}$$

where $A_m = \sqrt{2\pi}e^{-j(\pi/4)}(\phi_m(z_s)\phi_m(z_r)/\sqrt{k_m r_i})$. To improve the SNR, beamforming is performed on the signal received on the HLA at the ith moment. For conventional beamforming, the output of beamforming is written as

$$B(\widehat{\theta}_i) = \frac{1}{2L+1}\sum_{l=-L}^{L} e^{jkld\sin\widehat{\theta}_i} p_l(r_i, z_r). \tag{3}$$

After substituting (2) into (3), let $X_m = -(k_m - j\alpha_m)\sin\theta_i + k\sin\widehat{\theta}_i$, and we obtain

$$\begin{aligned} B(\widehat{\theta}_i) &= \frac{1}{2L+1}\sum_{m=1}^{M} A_m e^{-jk_m r_i - \alpha_m r_i}\sum_{l=-L}^{L} e^{jldX_m} \\ &= \frac{1}{2L+1}\sum_{m=1}^{M} A_m e^{-jk_m r_i - \alpha_m r_i}\frac{\sin[(L+1/2)dX_m]}{\sin((d/2)X_m)}. \end{aligned} \tag{4}$$

The estimation of the look direction $\widehat{\theta}_i$ can be obtained by many methods [14]. In order to explain the algorithm conveniently, we discuss the method of estimating the sound source depth when source moves away from the HLA under the assumption that $\widehat{\theta}_i = \theta_i = \theta$.

2.1. Wavenumber Estimation Using Generalized Hankel Transform. In range-independent shallow water waveguides, a Hankel transform pair presents the relationship between the complex pressure field $p(r; z_s, z_r)$ and the Green's function $g(k_r; z_s, z_r)$ [15]

$$\begin{aligned} p(r; z_s, z_r) &= \int_0^{+\infty} g(k_r; z_s, z_r) J_0(k_r r) k_r dk_r \\ g(k_r; z_s, z_r) &= \int_0^{+\infty} p(r; z_s, z_r) J_0(k_r r) r dr, \end{aligned} \tag{5}$$

where J_0 is the zeroth-order Bessel function.

Considering the computation of Hankel transform, the Green's function is often approximated by an inverse Fourier transform (FT) as [15]

$$g(k_r; z_s, z_r) \sim \frac{e^{i(\pi/4)}}{\sqrt{2\pi k_r}}\int_{-\infty}^{+\infty} p(r; z_s, z_r) e^{ik_r r}\sqrt{r} dr, \quad k_r r \gg 1. \tag{6}$$

We consider the source motion model, source range $= r_i = r_0 + iv\Delta t$, where Δt is the sampling interval and r_0 is the unknown initial source range at $t = 0$. We assume that the source radiates a tone signal and the source speed v is known as *a priori* [7, 12, 13]. According to (6), the Hankel transform, which is used previously to estimate the wavenumber, requires knowledge of the source range. Therefore, we apply the generalized Hankel transform [7] to the beamforming output. The generalized Hankel transform for the beamforming output is described as

$$\overline{g}(k_r, z_r) = \frac{e^{i(\pi/4)}}{\sqrt{2\pi k_r}}\int_{r_0}^{r_0+R} B(r) e^{ik_r r} S(r) dr, \quad k_r r_0 \gg 1, \tag{7}$$

where R is the range span wherein source moves during the observation time. $S(r)$ is intended to compensate for the cylindrical spreading loss and will be obtained directly from the data.

$$S(r) = \left\langle |B(r)|^2 \right\rangle^{-1/2}, \tag{8}$$

where $\langle\,\rangle$ is the range averaging or smoothing operation. Equation (7) reduces to the original Hankel transform by setting $S(r) = \sqrt{r}$. In the present discussion, $S(r)$ is approximately proportional to $\sqrt{r}$ using range averaging. After substituting (4) into (7), while assuming $S(r) \sim \sqrt{r}$, we obtain

$$\begin{aligned} &\overline{g}(k_r, z_r) \\ &\sim \sum_{m=1}^{M}\frac{\phi_m(z_s)\phi_m(z_r)}{\sqrt{k_r k_m}}\sin b(X_m)\int_{r_0}^{r_0+R} e^{j(k_r-k_m)r-\alpha_m r} dr \\ &= \sum_{m=1}^{M} a_m \frac{\phi_m(z_s)\phi_m(z_r)}{k_r - k_m + j\alpha_m}, \end{aligned} \tag{9}$$

where

$$a_m = \frac{e^{j[(k_r-k_m)-\alpha_m](r_0+R)} - e^{j[(k_r-k_m)-\alpha_m]r_0}}{j\sqrt{k_r k_m}}\sin b(X_m). \tag{10}$$

When $k_r = k_m$, the value of the mth item is much larger than the others in (9). Therefore, the wavenumber spectral peak at $k_r = k_m$ is given by

$$\overline{g}(k_m, z_r) \sim b_m \phi_m(z_r), \tag{11}$$

$$b_m = \frac{2e^{-\alpha_0 r'}}{\alpha_m k_m}\sinh\left(\frac{\alpha_m R}{2}\right)\phi_m(z_s)\sin b(X_m), \tag{12}$$

where $r' = r_0 + R/2$. This expression can be described by the matrix form.

$$\mathbf{g} = \mathbf{\Phi}\cdot\mathbf{b}, \tag{13}$$

where

$$\mathbf{g} = [\overline{g}(k_1, z_r), \overline{g}(k_2, z_r), \ldots, \overline{g}(k_M, z_r)]^T, \tag{14}$$

$$\mathbf{\Phi} = \mathrm{diag}([\phi_1(z_r), \phi_2(z_r), \ldots, \phi_M(z_r)]), \tag{15}$$

$$\mathbf{b} = [b_1, b_2, \ldots, b_M]^T, \tag{16}$$

The aforementioned wavenumber estimation method is based on the FT and is convenient to be calculated by

FFT. However, the FT-based approach presets some inherent disadvantages: (1) the spectral resolution of FT is limited by the range span. To resolve the modal wavenumbers between the ith and jth modes, the range needs to be larger than the interference distance, that is, $d_{ij} = 2\pi/|k_i - k_j|$. If all the wavenumbers are estimated, then the range must be larger than all interference distances. (2) The spectrum leakage occurs seriously when the method is applied to the data with a short range span. The sidelobes of strong spectral components can contaminate the weak spectral components or generate a false spectral peak. With the increase in source frequency or waveguide depth, the lower mode wavenumbers will closely group together. As a result, the wavenumbers are difficult to be estimated in this environment. Considering the drawbacks of FT, the modern spectral estimation methods can be applied to wavenumber estimation.

2.2. Wavenumber Estimation Using AR Model. Several methods have been developed to extract the mode wavenumbers, such as Prony's method, the signal subspace algorithms, and matrix-pencil [16, 17]. However, these methods regard the number of wavenumbers as *a priori*. The number of wavenumbers cannot be known correctly in practice. The AR spectral estimators based on an all-pole model are often used to extract the spectral peaks in frequency estimation [18]. The AR estimator does not need to know the number of wavenumbers and is thus attractive to estimate wavenumbers. However, the source range must be known for the AR estimator. Consequently, improved AR estimator should be used to extract the mode wavenumbers.

The method can be divided into three steps. First, data are preprocessed by

$$y[i] = B(r_i)\, S(r_i) \quad i = 1, 2 \ldots 2L + 1 \tag{17}$$

Second, considering that $y[i]$ can be described as the output of a linear system, we construct the AR model as

$$y[i] = -\sum_{k=1}^{p} a[k]\, y[i-k] + u[i], \tag{18}$$

where p is the order of the AR model to represent the data and is often set to $(2/3)(2L + 1)$ [18]. Finally, we assume that $u[i]$ is a zero mean white noise sequence with σ^2. Therefore, the wavenumber spectral density P_{AR} is expressed as

$$P_{AR}(l) = \frac{\sigma^2}{\left|1 + \sum_{k=1}^{p} a[k] \exp[-ilk]\right|}. \tag{19}$$

P_{AR} is obtained by estimating the coefficients $a[1], a[2], \ldots, a[p]$ and σ^2. The above-mentioned coefficients can be estimated in different ways. We select the modified covariance approach because it avoids the spectral line splitting effectively [18]. The locations of peaks in P_{AR} yield the wavenumbers estimated by AR model. The peak levels estimated by AR estimator possess large variances [18]. Therefore, AR estimator is unsuitable to estimate the modal amplitudes.

3. Matched-Mode Source Depth Estimation

As discussed above, the wavenumbers can be estimated by AR spectrum. However, AR spectrum is unsuitable to estimate the modal amplitudes. The performance of estimating wavenumbers degrades by using the generalized Hankel transform. The performance is affected by false spectral peaks and spectral resolution. To combine the advantages of two methods, the modal amplitudes are estimated by generalized Hankel transform with a prior knowledge of wavenumbers that are estimated by AR model. Therefore, we estimate the wavenumber k_m by AR model and then obtain $\overline{g}(k_m, z_r)$ in the wavenumber spectrum on the basis of the generalized Hankel transform.

According (13), we use a source depth ambiguity function to estimate source depth, and this function is expressed as

$$D(z) = \boldsymbol{\varphi}(z)\, \boldsymbol{b}\boldsymbol{b}^{\boldsymbol{H}} \boldsymbol{\varphi}^{\boldsymbol{H}}(z), \tag{20}$$

where

$$\boldsymbol{\varphi}(z) = [\phi_1(z), \phi_2(z), \ldots, \phi_M(z)]. \tag{21}$$

$\boldsymbol{b}$ can be solved by

$$\boldsymbol{b} = (\boldsymbol{\Phi} + \boldsymbol{U})^{-1} \boldsymbol{g}, \tag{22}$$

$$\boldsymbol{U} = \operatorname{diag}\left(\left[\frac{\Delta}{\phi_1(z_r)}, \frac{\Delta}{\phi_2(z_r)}, \ldots, \frac{\Delta}{\phi_M(z_r)}\right]\right). \tag{23}$$

where Δ is a small amount (on the order of one-half of the maximum value of the mode function) for preventing the singularity of $\boldsymbol{\Phi}$. Wavenumbers k'_m and $\phi_m(z)$ are calculated by KRAKEN on the basis of a given frequency and environmental information (SSP and bottom properties). Some modes cannot be resolved even if we use the AR spectrum, such that the number of $\overline{g}(k_m, z_r)$ is less than M. We assume that only M_0 order is estimated. $\phi_m(z)$ with the same order of $\overline{g}(k_m, z_r)$ can be determined by solving the problem as follows:

$$\begin{aligned} &\min \quad (\boldsymbol{k} - \boldsymbol{k}_0)^{\boldsymbol{H}} (\boldsymbol{k} - \boldsymbol{k}_0) \\ &s.t. \quad \boldsymbol{k}_0(1) < \boldsymbol{k}_0(2) < \cdots < \boldsymbol{k}_0(M_0), \end{aligned} \tag{24}$$

where

$$\boldsymbol{k} = \left[k_1, k_2, \ldots, k_{M_0}\right]^T, \tag{25}$$

$$\boldsymbol{k}' = \left[k'_1, k'_2 \ldots, k'_M\right]^T, \tag{26}$$

$$\boldsymbol{k}_0 \subseteq \boldsymbol{k}'. \tag{27}$$

$\boldsymbol{k}$ is an $M_0 \times 1$ vector, $\boldsymbol{k}'$ is an $M \times 1$ vector, and $\boldsymbol{k}_0$ is an $M_0 \times 1$ vector.

4. Numerical Simulation

4.1. Depth Estimation in Exactly Known Environment. This section presents comparisons of the source depth estimation results of the SAB and the proposed matched-mode

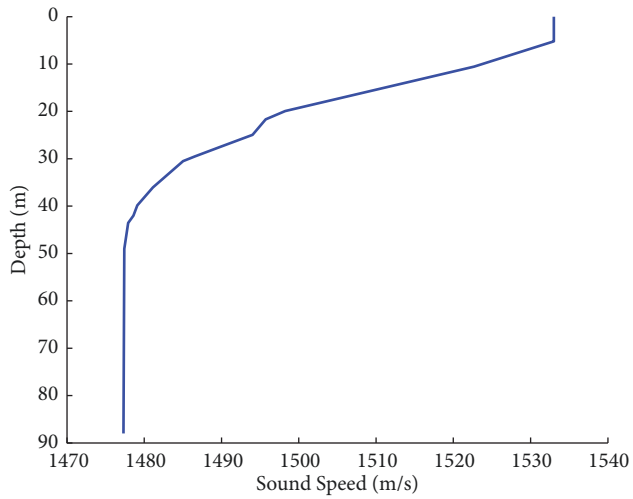

Figure 2: Sound speed profile.

autoregressive depth estimation method (MMAR) in a series of realistic test cases. For SAB, source depth can be estimated using only a single hydrophone under the assumption that source moves away from receiver at a constant speed during the observation time. For convenient comparison, we assume the source of SAB moves along the beam direction of HLA.

The pressure field is generated using the KRAKEN program. The SSP for simulation is shown in Figure 2, and the bottom properties are referred to [7]. The considered HLA possesses $2L + 1$ receivers that are uniformly spaced with d, where $d = \lambda/2$, $L = 5$. The HLA depth is 70 m. In studying the difference in depth estimation performance, we consider two sources depths of 4 and 50 m, which correspond to shallow and deep sources, respectively. The initial source range is 5010 m, but this information is assumed to be unknown. The performance influenced by the unknown initial source range has been discussed in [7]. We assume that each source moves away from the HLA with a speed of 2.5 m/s and radiates the narrowband signal with 350 Hz. To compiling the source depth estimation results, three different SNRs of 20, 5, and -5 dB are considered, where the SNR is defined as

$$SNR = 10\lg\frac{P_s}{P_n}\bigg|_{r=r_0}. \tag{28}$$

According to (28), when source range is 5010 m, the SNR is described by the ratio of signal power P_s and noise power P_n at receiver. The array gain is already considered in SNR. Source depth estimation results are also compiled for different range spans (insufficient and sufficient range span).

Before examining the source depth estimation, it is necessary to consider the wavenumber estimation results for different range spans and SNRs. A unified description is given to avoid duplication; that is, the deep source is expressed by the blue line and the shallow source is expressed by the red line. Figure 3 shows the wavenumber estimation with a sufficient range span (4990 m) for different SNRs. Figures 3(a), 3(c), and 3(e) show that the wavenumbers are estimated by the method in SAB with SNR = 20, 5, and -5 dB. With the decreasing SNR, spectral peaks are more difficult to identify accurately. When the SNR is around -5 dB, too many false spectral peaks are identified as the true ones. For example, there is no true spectral peak from range 1.3–1.36 in wavenumber domain. However, the false spectral peaks are identified as true ones in Figure 3(e), because the levels of false spectral peaks are high (especially for the deep source). Figures 3(b), 3(d) and 3(f) show that the wavenumbers are estimated by the proposed wavenumber estimation method with SNR = 20 dB, 5 dB, and -5 dB. Compared with Figure 3(e), the number of false spectral peaks, which are identified as the true ones, is obviously decreased in Figure 3(f).

Figure 4 shows the wavenumber estimation with the insufficient range span (1990 m) for different SNRs. Comparing Figures 3(a), 3(c), and 3(e) with Figures 4(a), 4(c), and 4(e), we see that when the range span is insufficient, wavenumber spectrum in SAB is more broadening. It makes more difficult to identify the spectral peaks. Comparing Figure 4(b) with Figure 4(a), the spectral peaks can be identified more easily, because the proposed method has a higher resolution.

Figure 5 shows the source depths are estimated by SAB and MMAR with a sufficient range span for different SNRs. From Figures 5(a) and 5(b), both SAB and MMAR can estimate source depths accurately, whether the source is shallow or deep. With the decreasing SNR, the source depth estimation results are obviously worse by using SAB as shown in Figures 5(c) and 5(e). The main reason for the bad depth estimation is the false spectral peak problem, which is discussed in Figure 3. Compared with the depth estimation in Figures 5(c) and 5(e), MMAR can estimate source depths effectively for SNR = 5 and -5 dB as shown in Figures 5(d) and 5(f).

Figure 6 shows the source depths are estimated by SAB and MMAR with an insufficient range span for different SNRs. Since the spectral peaks are difficult to identify, SAB fails to estimate source depth as shown in Figures 6(a), 6(c), and 6(e). When SNR is high (20 dB), MMAR can estimate

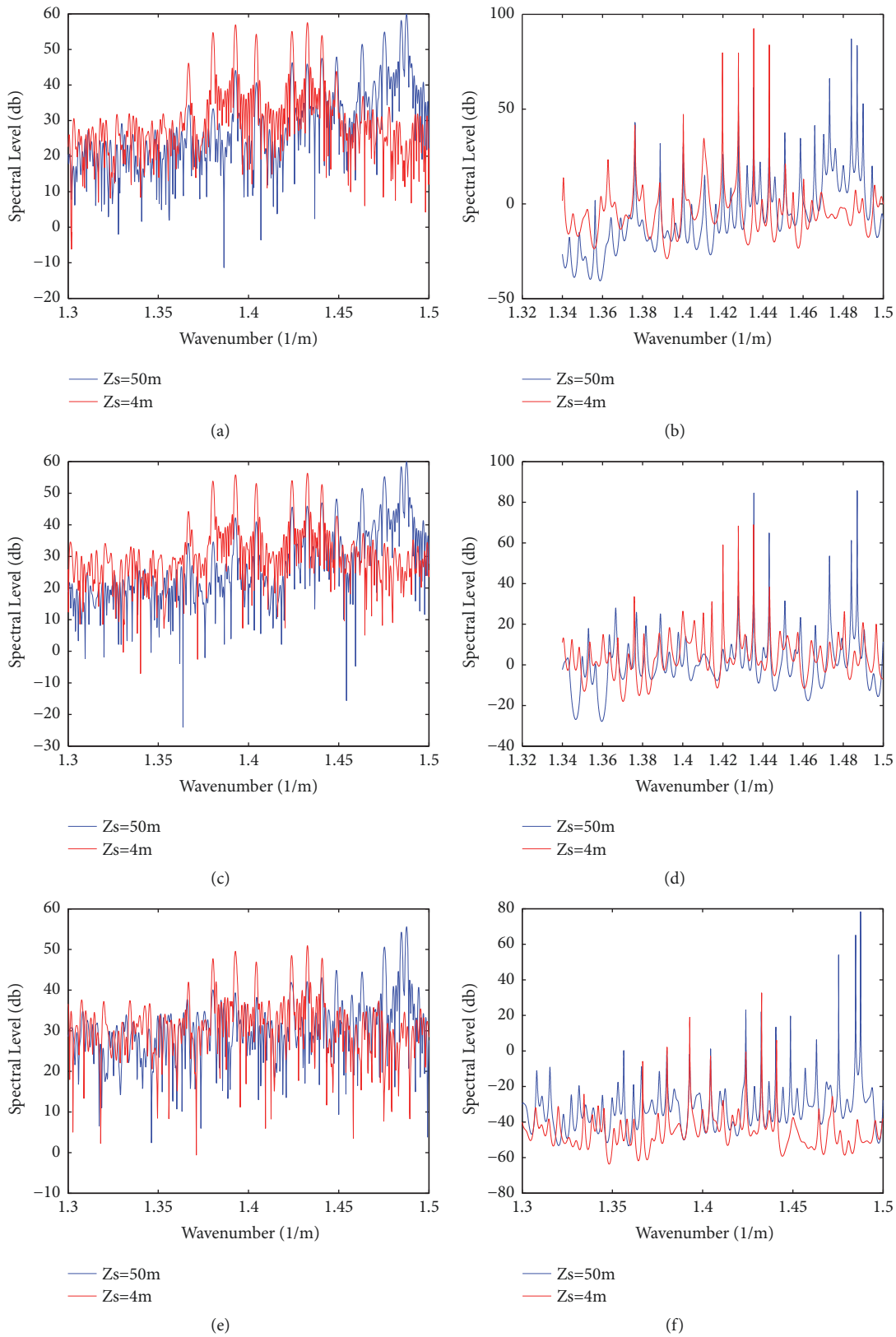

Figure 3: Wavenumber spectrum estimation with a sufficient range span at 350 Hz. The wavenumber estimation methods in SAB with SNR = 20, 5, and -5 dB are shown in (a), (c), and (e), respectively. The wavenumber estimation methods proposed in this paper with SNR = 20, 5, and -5 dB are shown in (a), (c), and (e), respectively.

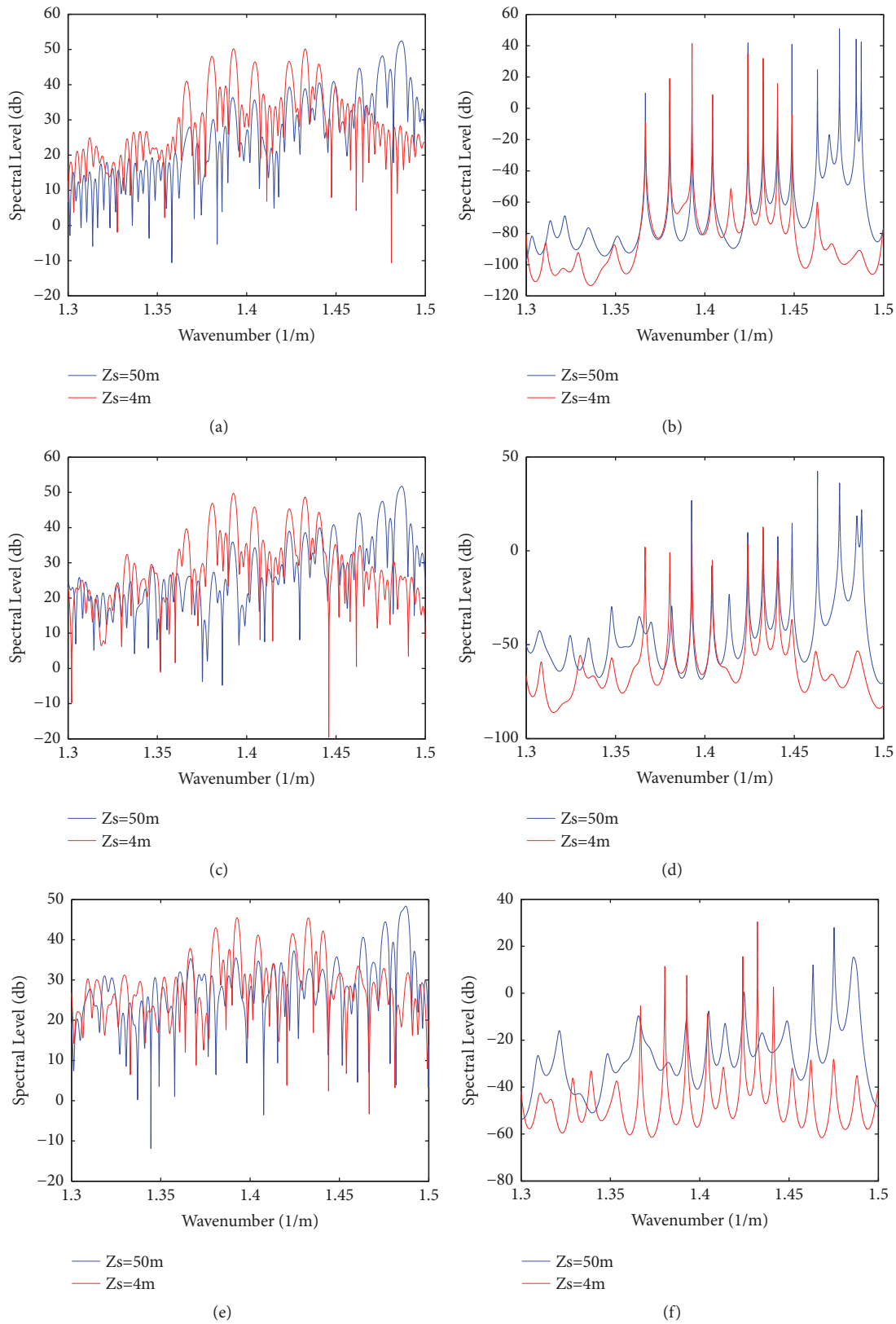

Figure 4: Wavenumber spectrum estimation with an insufficient range span at 350 Hz. The wavenumber estimation methods in SAB with SNR = 20, 5, and -5 dB are shown in (a), (c), and (e), respectively. The wavenumber estimation methods proposed in this paper with SNR = 20, 5, and -5 dB are shown in (a), (c), and (e), respectively.

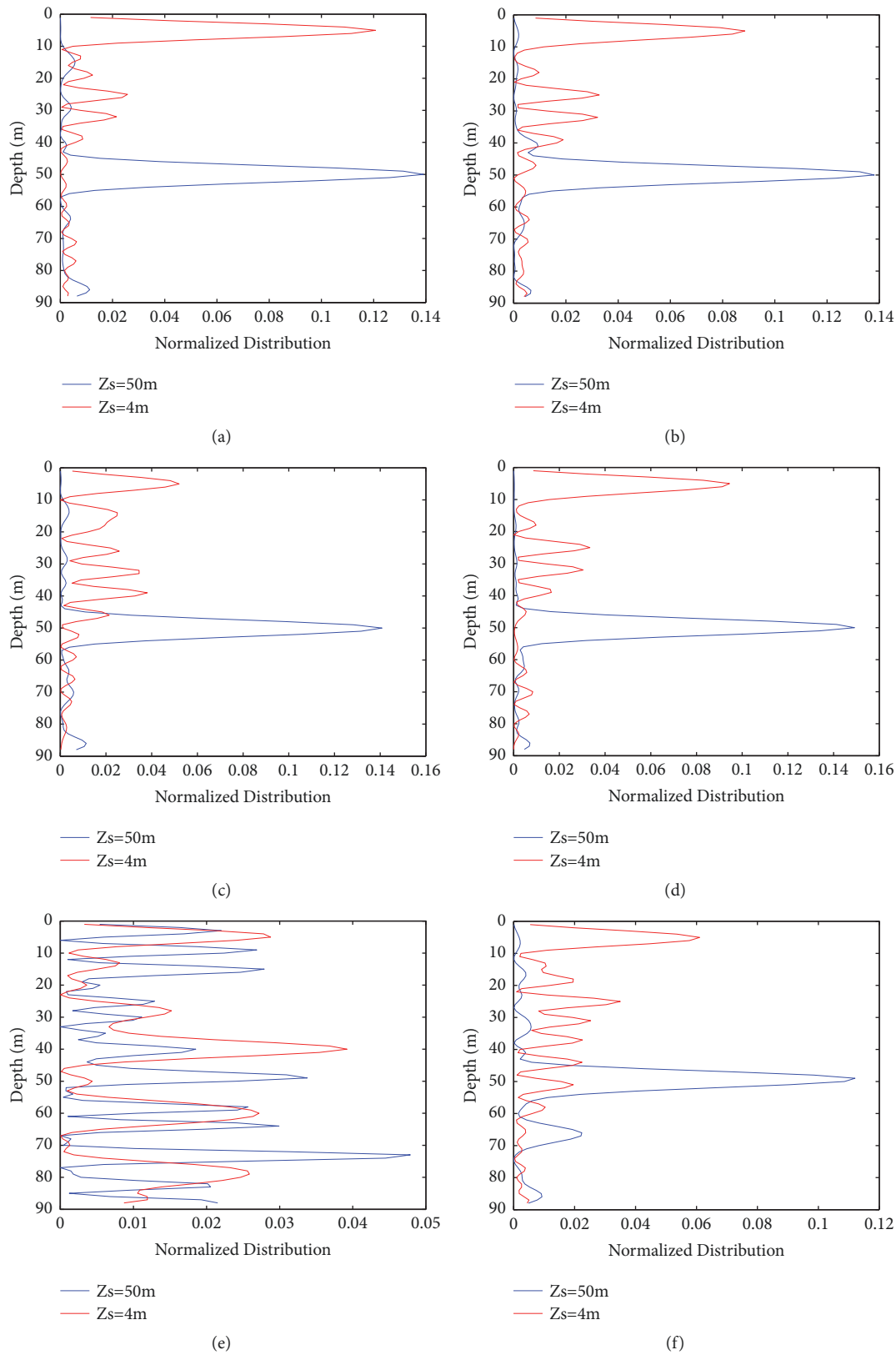

Figure 5: Normalized depth ambiguity functions with a sufficient range span for the shallow (Zs = 4 m) and deep (Zs = 50 m) sources. Source depths are estimated by SAB with SNR = 20 dB, 5 dB, and -5 dB in (a), (c), and (e), respectively. Source depths are estimated by MMAR with SNR = 20 dB, 5 dB, and -5 dB in (b), (d), and (f), respectively.

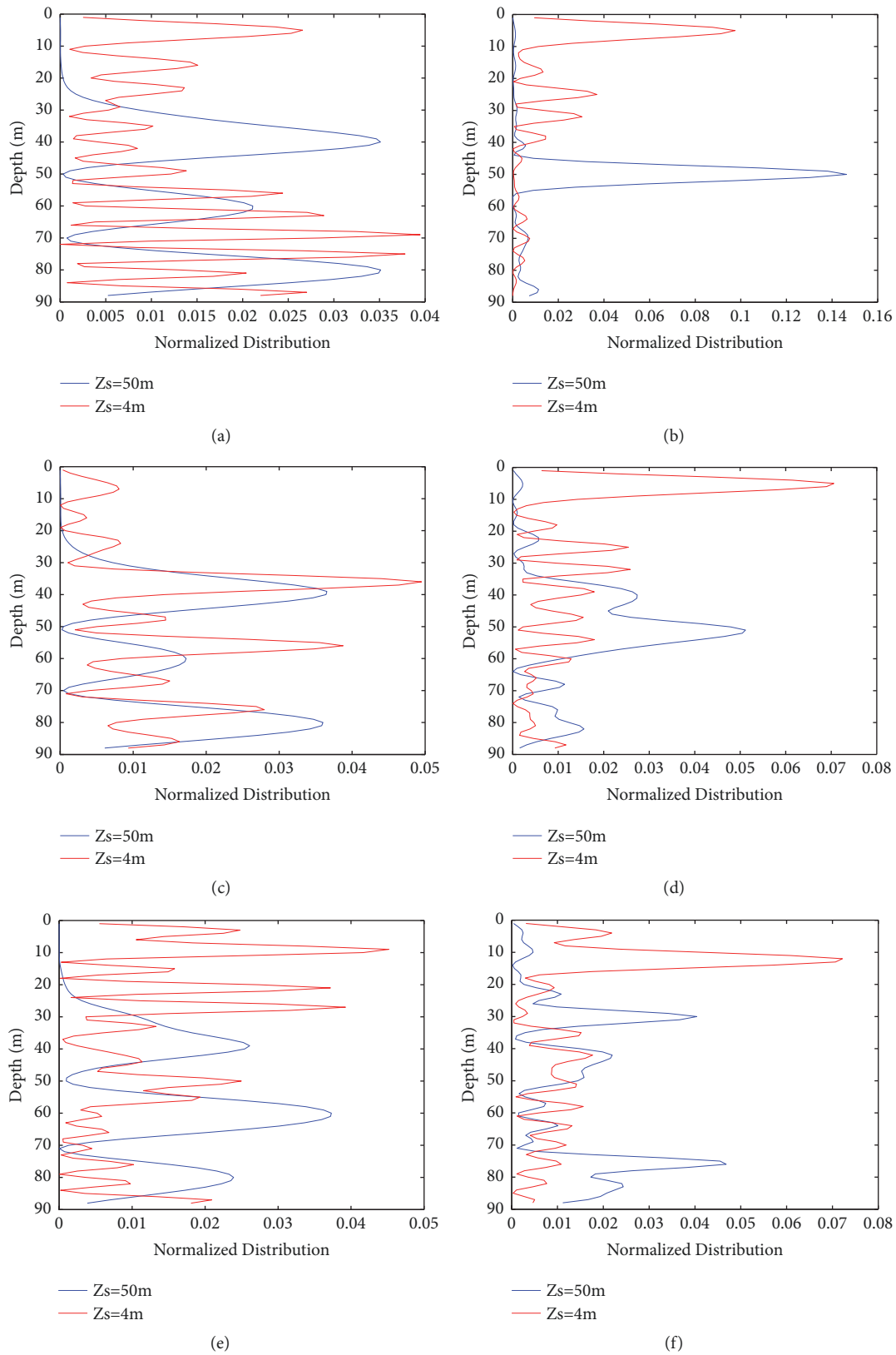

Figure 6: Normalized depth ambiguity functions with an insufficient range span for the shallow (Zs = 4 m) and deep (Zs = 50 m) sources. Source depths are estimated by SAB with different SNR in (a), (c), and (e). Source depths are estimated by MMAR with different SNR in (b), (d), and (f).

source depth accurately, whether the source is shallow or deep. When SNR decreases to 5 dB, MMAR can also estimate the shallow source depth. However, the deep source depth is estimated with a bias. Figure 6(d) shows the false spectral peaks have high spectral levels, which make difficult to identify the true spectral peaks. When SNR decreases to -5 dB, MMAR fails to estimate the deep source depth and estimates the shallow one with a bias as shown in Figure 6(f), because false spectral peaks in wavenumber spectrum of deep source have higher spectral level than that of shallow ones.

The depth estimation results in Figures 5 and 6 are for a single realization of random noise on the data. To obtain meaningful general comparisons between the two depth estimation methods, 500 independent random noise realizations are added to the acoustic signal for $z_s = 50 \ m$. The performance of the two methods is quantified the estimated probability of correct depth P, which is defined as

$$P = \frac{C}{C_0}, \tag{29}$$

where C is the times that the estimated source depth within a suitably small region about the true depth. The small region is defined as $\pm 5 \ m$ in depth in this paper. C_0 is the total number of the realizations. In this paper, $C_0 = 500$. Ninety-percent confidence intervals for the probability of correct localization are [19]

$$\left[P - 1.645\sqrt{\frac{P(1-P)}{C_0}}, P + 1.645\sqrt{\frac{P(1-P)}{C_0}} \right]. \tag{30}$$

The estimated probabilities of correct depth for SAB and MMAR for known environment with error bars denoting 90% confidence limits are shown in Figure 7. Figures 7(a), 7(b), and 7(c) are corresponding to SNRs of 20, 5, and -5 dB, respectively. Figure 7(a) shows that, at SNR = 20 dB with 4490 m –4990 m range span, both methods yield a high estimated probability of correct depth. However, with a range span from 1990 m to 3990 m, MMAR has an obviously higher probability than SAB. Figure 7(b) shows that MMAR performs well for 2490 m or larger range span, when SNR = 5 dB. Figure 7(c) shows that, for SNR = -5 dB, MMAR estimates depth well for 2990 m or larger range span.

4.2. Depth Estimation in Mismatch Environment. In Section 4.1, it has been assumed that the environmental parameters are known exactly for all depth estimation examples. In practical applications, the properties of the environment (water-column sound speed profile (SSP) and seabed geoacoustic parameters) are not known exactly. We focus on the performance of MMAR and SAB in mismatch environment in this Section. We discuss the performance of MMAR and SAB with SSP mismatch, seabed geoacoustic parameters mismatch, and the combination of SSP mismatch and seabed geoacoustic parameters mismatch in Sections 4.2.1, 4.2.2, and 4.2.3, respectively. The acoustic data considered in this Section were generated by KRAKEN using the environment model described in Section 4.1. The matched modes are computed for the environment with different types of mismatches (SSP mismatch, seabed geoacoustic parameters mismatch and combination of SSP mismatch, and seabed geoacoustic parameters mismatch). The performance of the proposed method is evaluated by carrying out Moute Carlo sampling over random realizations of environmental mismatches.

4.2.1. Sound Speed Profile Mismatch. Adding the random perturbation to the SSP depth by depth, the additive perturbation is modeled as zero-mean Gaussian processes. The standard deviations of the perturbations are 5 m/s and 10 m/s, which are denoted by $\delta = 5$ m/s and $\delta = 10$ m/s, respectively. As in Section 4.1, depth estimation results for MMAR and SAB are considered for three SNRs (20, 5 and -5 dB). Figure 8 shows how the probabilities of correct estimated depth vary with the range span for these cases. In comparing Figure 8 with Figure 7 (no mismatch), it is clear that the probability of correct depth estimation decreases with SSP mismatch, in some cases (such as Figures 8(b), 8(d), 8(e), and 8(f)) by a substantial amount. Comparing the performance of MMAR with that of SAB, the results of MMAR are generally superior to that of SAB in Figure 8. Also, from Figures 8(a), 8(c), and 8(e) or 8(b), 8(d) and 8(f), we can see that the probability of correct depth estimation based on MMAR and SAB decreases with SNR.

4.2.2. Seabed Geoacoustic Properties Mismatch. Seabed geoacoustic properties mismatch includes mismatches of sediment sound speed, density, and attenuation. The density and attenuation of sediment have few effects on the stability of MFP [20]. The conclusion can be obviously extended to MMAR and SAB. Therefore, we focus on the effects of sediment sound speed mismatch on the performance of MMAR and SAB.

Also a random perturbation is added to the sediment sound speed, which is considered as the mismatch of sediment sound speed. The standard deviations of additive perturbation are 30 m/s and 50 m/s, which are denoted by $\Delta = 30$ m/s and $\Delta = 50$ m/s, respectively. As in the previous section, depth estimation results for MMAR and SAB are considered for three SNRs with different range span. Figure 9 shows that the probabilities of correct depth estimation for those cases with different sediment sound speed mismatch. Like the discussion in Section 4.2.1, the probabilities of correct depth estimation decrease with varying the mismatch of sediment sound speed. From Figure 9, it is apparent that as SNR decreases the depth estimation results for two methods degrade, regardless of the range span. One should note that although the magnitude of sediment sound speed mismatch is larger than that of SSP mismatch, the performance of the two methods in sediment sound speed mismatch case is better than that in SSP mismatch cases. It means that the two methods are more sensitive to the SSP mismatch than sediment sound speed mismatch.

4.2.3. Environmental Mismatch. For the realistic scenarios, the environmental mismatch is always complicated. Therefore, we consider the environmental mismatch, which combines SSP mismatch and seabed sound speed mismatch.

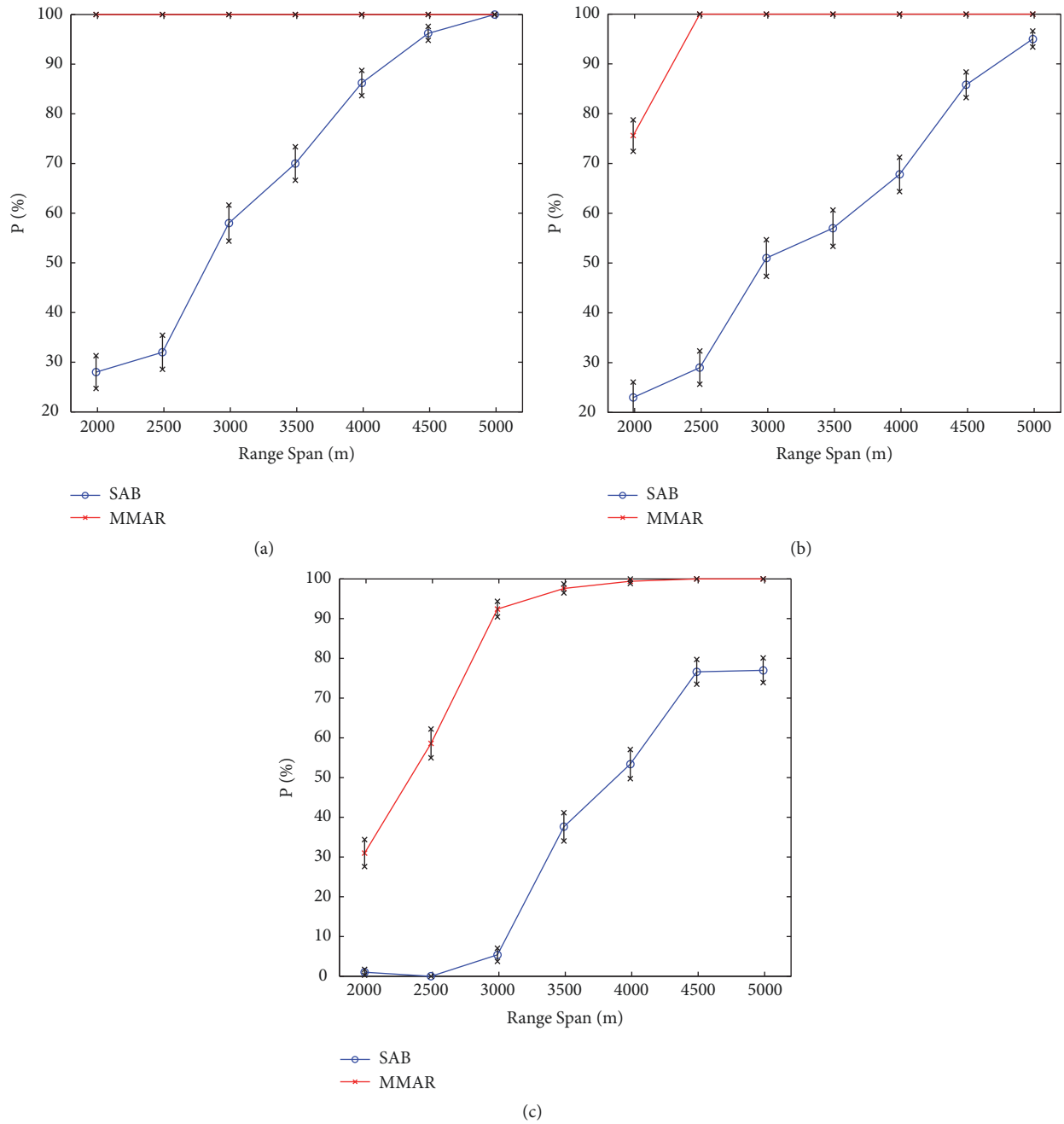

Figure 7: Estimated probability of correct depth P with known environmental parameters for SAB (the blue line with open circles) and MMAR (the red line with crosses). (a), (b), and (c) give results with different range spans (from 1990 m to 4990 m) at SNRs of 20, 5, and -5 dB, respectively.

Compared with Figures 8 and 9, the performance of the two method decreases in Figure 9 as another mismatch exists. Also, the performance of MMAR is generally superior to that of SAB in Figure 10. When the environmental mismatch is relatively large as shown in Figures 10(b), 10(d), and 10(f), two methods fail to work. When the environmental mismatch is relatively small as shown in Figures 10(a), 10(c), and 10(e), the estimated probability of MMAR is relatively high at relatively high SNR (SNR= 20 and 5 dB). Even if SNR is low, MMAR can estimate source depth effectively with relatively large range span.

5. Summary and Discussion

A matched-mode method based on AR using an HLA to estimate the moving source depth is developed in this study. The modal wavenumber spectrum is obtained using generalized Hankel transform with the data from the moving source. The mode amplitudes can be extracted by combining the information based on AR modal wavenumber spectrum and the FT wavenumber spectrum. The amplitudes contain the information of source depth. The source depth is estimated by matching the mode

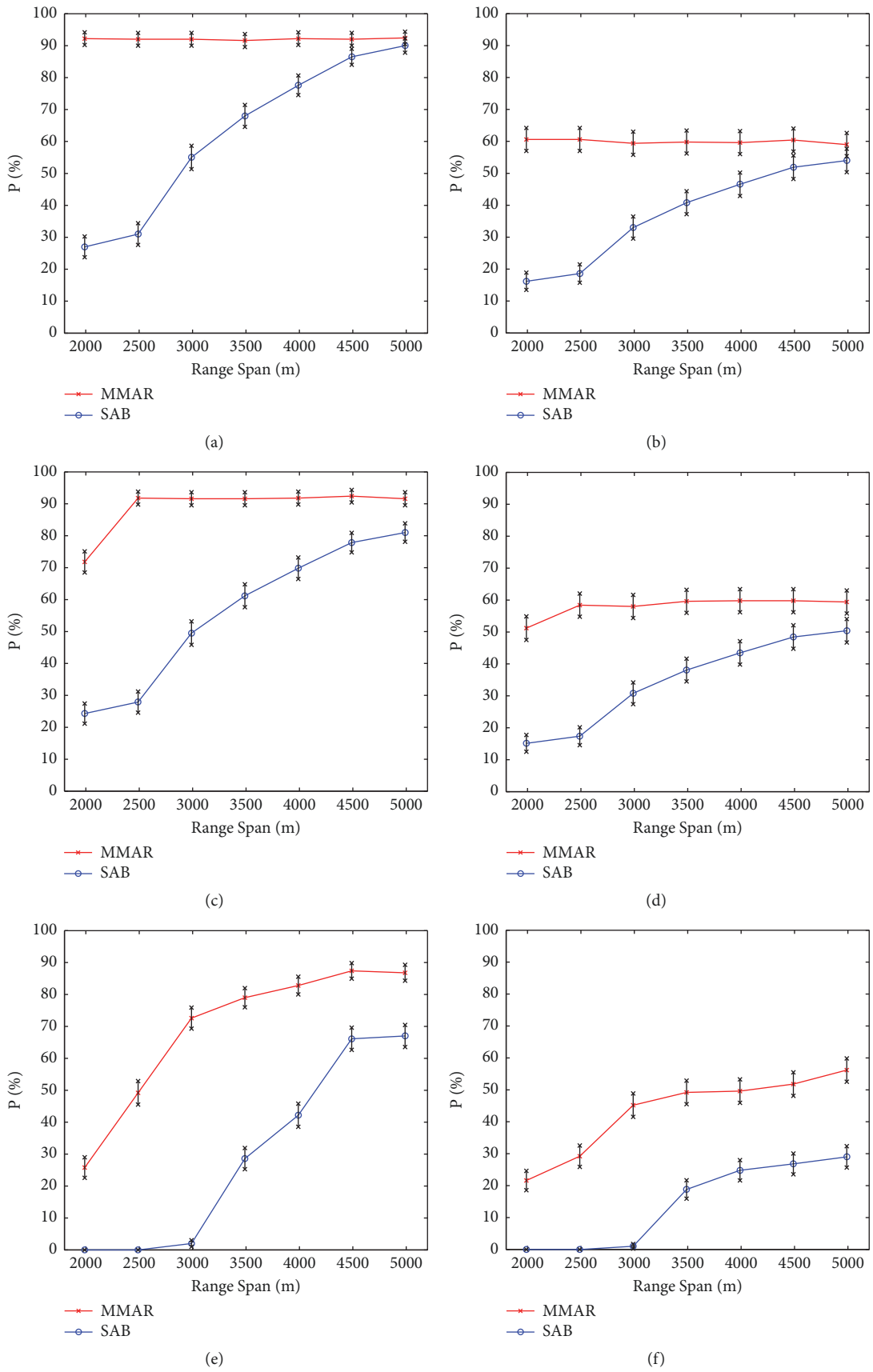

FIGURE 8: Estimated probability of correct depth P with SSP mismatch for MMAR (red cross) and SAB (blue open circle). (a), (c), and (e) give results for SSP mismatch $\delta = 5 \quad m/s$ cases at SNRs of 20, 5, and -5 dB, respectively; (b), (d), and (f) give results for SSP mismatch $\delta = 10 \quad m/s$ cases at the same SNRs. Error bars denote 90% confidence intervals.

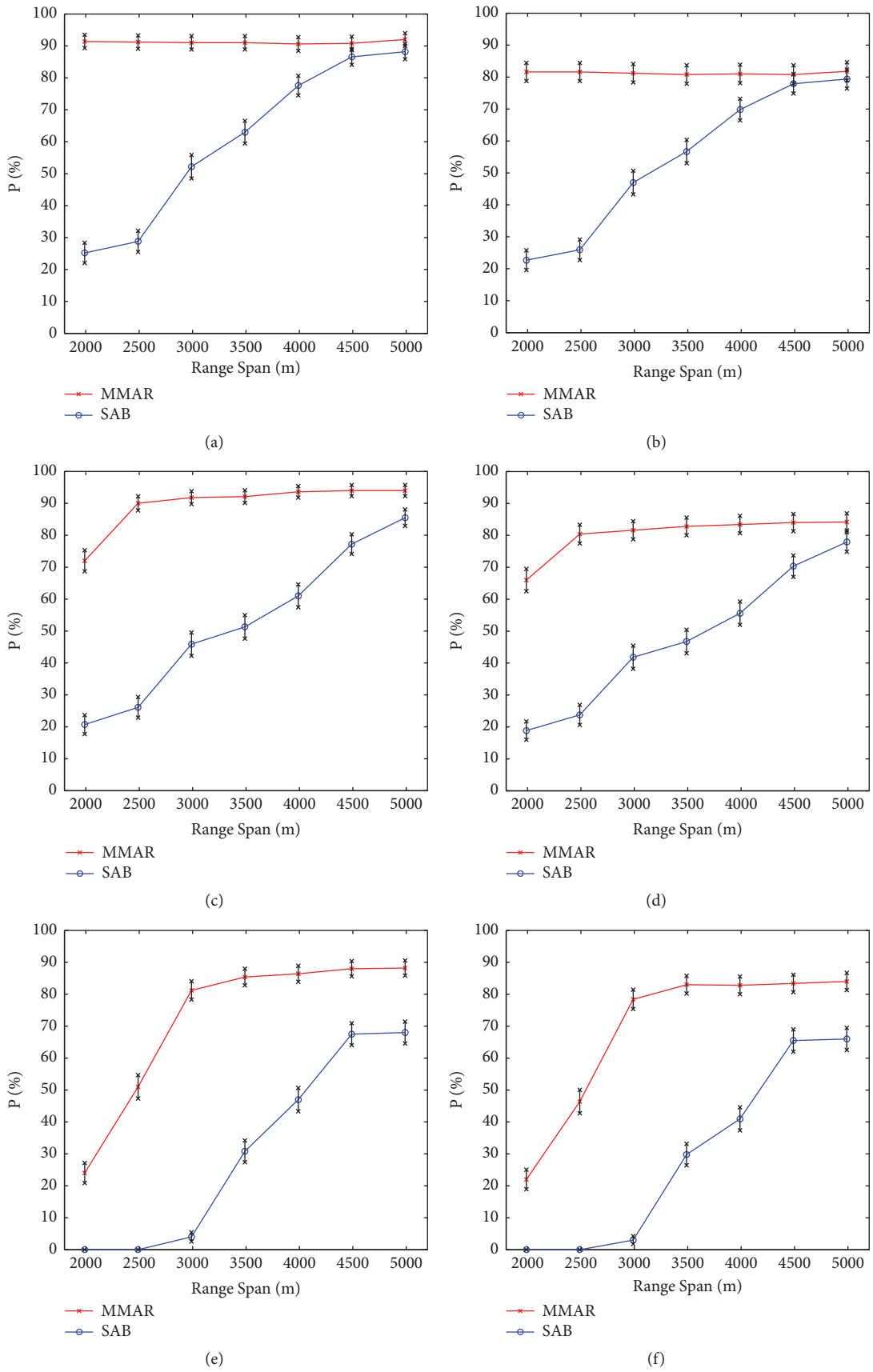

FIGURE 9: Estimated probability of correct depth P with seabed geoacoustic properties mismatch for MMAR (red cross) and SAB (blue open circle). (a), (c), and (e) give results for seabed geoacoustic properties mismatch $\Delta = 30 \quad m/s$ cases at SNRs of 20, 5, and -5 dB, respectively; (b), (d), and (f) give results for seabed geoacoustic properties mismatch $\Delta = 50 \quad m/s$ cases at the same SNRs. Error bars denote 90% confidence intervals.

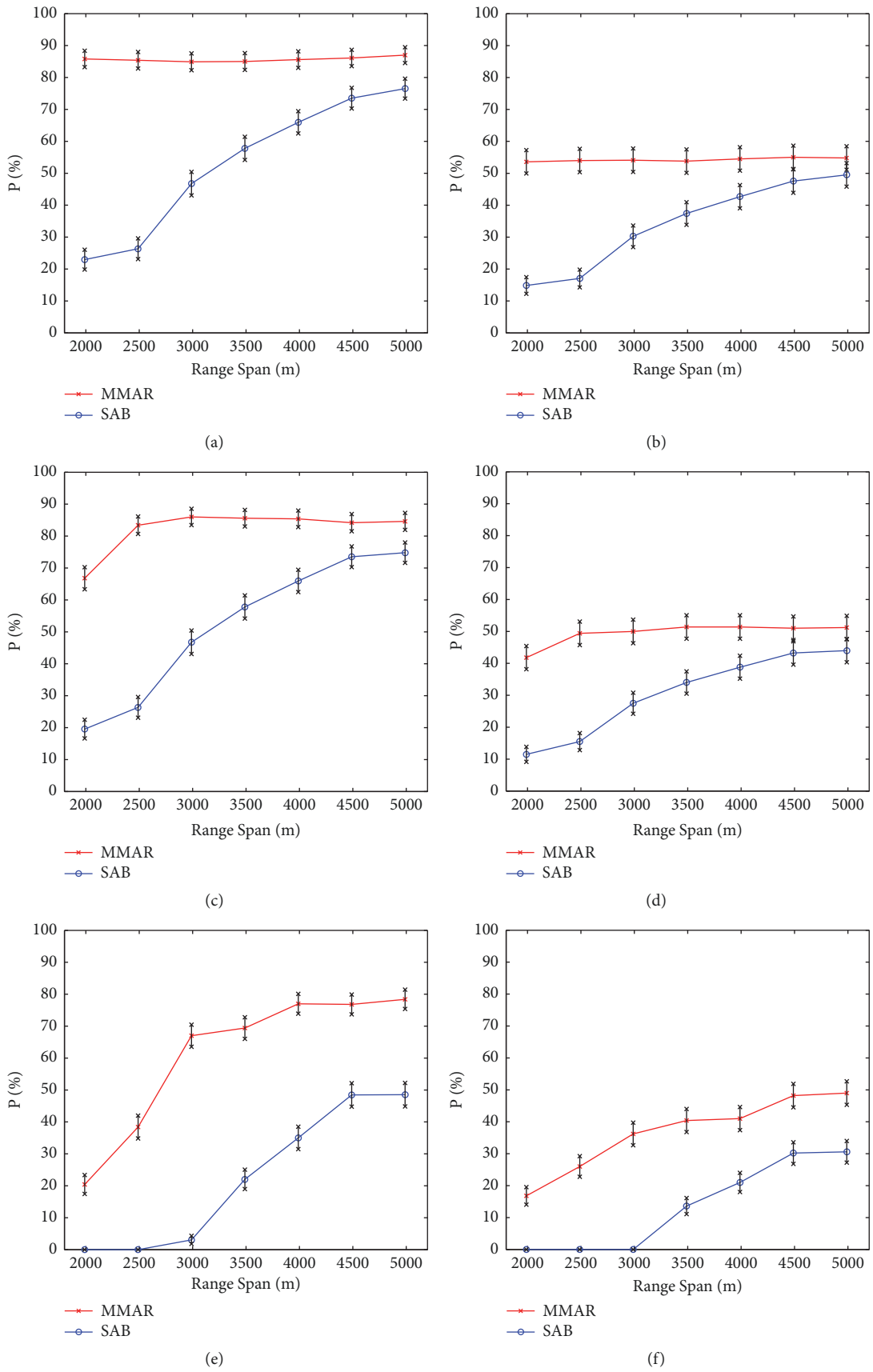

Figure 10: Estimated probability of correct depth P with environmental mismatch, which combines SSP and seabed sound speed mismatch, for MMAR (red cross) and SAB (blue open circle). (a), (c), and (e) give results for the combination of SSP mismatch $\delta = 5 \quad m/s$ and seabed geoacoustic properties mismatch $\Delta = 30 \quad m/s$ cases at SNRs of 20, 5 and -5 dB, respectively; (b), (d), and (f) give results for the combination of SSP mismatch $\delta = 10 \quad m/s$ and seabed geoacoustic properties mismatch $\Delta = 50 \quad m/s$ cases at the same SNRs. Error bars denote 90% confidence intervals.

estimation with the mode depth function calculated by the KRAKEN.

The method proposed in this study is evaluated using the simulated data. For the data with a small range span or low SNR, the proposed method can achieve source depth estimation with better performance than SAB. The performance of the proposed method is evaluated in mismatch environment. The proposed method performs better than SAB in different environmental mismatch cases. The proposed method is insensitive to the environmental mismatch.

Compared with that in SAB, the requirement of the moving source traveling range decreases in proposed method. The proposed method can also be applied to the data with low SNR and in environmental mismatch cases. However, this method is limited because it assumes the source depth fixed during the observation time. The effectiveness of this method degrades sharply, when the source depth varies rapidly. Therefore, additional work is needed for its future application in source depth tracking.

Data Availability

The data used to support the findings of this study are included within the article.

Conflicts of Interest

The authors declare that there are no conflicts of interest regarding the publication of this paper.

Acknowledgments

This work was supported by the National Key R&D Plan (2017YFC0306900), the National Natural Science Foundation of China (11504064 and 61405041), the Technology of Basic Scientific Research Project (JSJL2016604B003), and the Open Fund for the National Laboratory for Marine Science and Technology of QingDao (QNLM2016ORP0102).

References

[1] A. B. Baggeroer, W. A. Kuperman, and P. N. Mikhalevsky, "An overview of matched field methods in ocean acoustics," *IEEE Journal of Oceanic Engineering*, vol. 18, no. 4, pp. 401–424, 1993.

[2] X. Wang, M. Xu, H. Wang, Y. Wu, and H. Shi, "Combination of Interacting Multiple Models with the Particle Filter for Three-Dimensional Target Tracking in Underwater Wireless Sensor Networks," *Mathematical Problems in Engineering*, vol. 2012, Article ID 829451, 16 pages, 2012.

[3] P. N. Tran and K. D. Trinh, "Adaptive Matched Field Processing for Source Localization Using Improved Diagonal Loading Algorithm," *Acoustics Australia*, vol. 45, no. 2, pp. 325–330, 2017.

[4] Y. Le Gall, F.-X. Socheleau, and J. Bonnel, "Matched-field processing performance under the stochastic and deterministic signal models," *IEEE Transactions on Signal Processing*, vol. 62, no. 22, pp. 5825–5838, 2014.

[5] S. M. Jesus, M. B. Porter, Y. Stéphan, X. Démoulin, O. C. Rodríguez, and E. M. M. Ferreira Coelho, "Single hydrophone source localization," *IEEE Journal of Oceanic Engineering*, vol. 25, no. 3, pp. 337–346, 2000.

[6] S. B. Suppappola and B. F. Harrison, "Experimental matched-field localization results using a short vertical array and mid-frequency signals in shallow water," *IEEE Journal of Oceanic Engineering*, vol. 29, no. 2, pp. 511–523, 2004.

[7] T. C. Yang, "Source depth estimation based on synthetic aperture beamfoming for a moving source," *The Journal of the Acoustical Society of America*, vol. 138, no. 3, pp. 1678–1686, 2015.

[8] R. Duan, K. Yang, Y. Ma, and B. Lei, "A reliable acoustic path: Physical properties and a source localization method," *Chinese Physics B*, vol. 21, no. 12, pp. 276–289, 2012.

[9] N. Booth, P. Baxley, J. Rice et al., "Source localization with broad-band matched-field processing in shallow water," *IEEE Journal of Oceanic Engineering*, vol. 21, no. 4, pp. 402–412, 1996.

[10] P. A. Forero, P. A. Baxley, and L. Straatemeier, "A multitask learning framework for broadband source-location mapping using passive sonar," *IEEE Transactions on Signal Processing*, vol. 63, no. 14, pp. 3599–3614, 2015.

[11] J. Bonnel, G. Le Touze, B. Nicolas, and J. I. Mars, "Physics-Based Time-Frequency Representations for Underwater Acoustics: Power Class Utilization with Waveguide-Invariant Approximation," *IEEE Signal Processing Magazine*, vol. 30, no. 6, pp. 120–129, 2013.

[12] T. C. Yang, "Moving Source Localization And Tracking Based on Data," *Oceans*, pp. 2147-2147, 2014.

[13] T. C. Yang, "Data-based matched-mode source localization for a moving source," *The Journal of the Acoustical Society of America*, vol. 135, no. 3, pp. 1218–1230, 2014.

[14] A. Bereketli, M. B. Guldogan, T. Kolcak, T. Gudu, and A. L. Avsar, "Experimental results for direction of arrival estimation with a single acoustic vector sensor in shallow water," *Journal of Sensors*, vol. 2015, Article ID 401353, 10 pages, 2015.

[15] G. V. Frisk and J. F. Lynch, "Shallow water waveguide characterization using the hankel transform," *The Journal of the Acoustical Society of America*, vol. 76, no. 1, pp. 205–216, 1984.

[16] T. K. Sarkar and O. Pereira, "Using the matrix pencil method to estimate the parameters of a sum of complex exponentials," *IEEE Antennas and Propagation Magazine*, vol. 37, no. 1, pp. 48–55, 1995.

[17] P. Roux, D. Cassereau, and A. Roux, "A high-resolution algorithm for wave number estimation using holographic array processing," *The Journal of the Acoustical Society of America*, vol. 115, no. 3, pp. 1059–1067, 2004.

[18] J. Marple, *Digital spectral analysis with applications*, Prentice Hall Signal Processing Series, Prentice Hall, Inc., Englewood Cliffs, NJ, 1987.

[19] N. Collison and S. Dosso, "A comparison of modal decomposition algorithms for matched-mode processing," *Canadian Acoustics - Acoustique Canadienne*, vol. 28, no. 4, pp. 15–27, 2000.

[20] Y. Le Gall, F.-X. Socheleau, and J. Bonnel, "Performance Analysis of Single-Receiver Matched-Mode Localization," *IEEE Journal of Oceanic Engineering*, pp. 1–14, 2017.